ALGERIAN JOURNAL OF ENGINEERING AND TECHNOLOGY

Algerian Journal of Engineering and Technology
ISSN: 2716-9227 (Print)
EISSN: 2716-9278 (Online)
DOI: http://dx.doi.org/10.57056/ajet.v10i1.189
Arabi et al / vol. 10, n°1 - 2025

Original Article Open Access

Removal of total phenolic compounds from olive mill wastewater by adsorption on natural soils: characterization of adsorbents, classical and under microwave irradiation kinetic study

Arabi Malika[a]*, Elias Abdelhamid[b], Ait Younes Yasmine[c], Kamel Ziane[d], Mansouri Belkacem[e], Toumert Idir[e]

[a]*Division of Development of the Application of Nuclear Techniques, Algiers Nuclear Research Center, Algeria*
[b]*Faculty of Sciences, Mouloud MAMMERI University, Tizi-Ouzou, Algeria*
[c]*Resigned;* [d]*Retirement*
[e]*Technical Services and Research Support Division, Algiers Nuclear Research Center, Algeria*
* *Corresponding author.* E-mail address: m.arabi@crna.dz
Article history: Received 09 December 2024, Revised 25 February 2025, Accepted 26 February 2025

ABSTRACT

The removal of total phenolic compounds (TPC) from olive mill wastewater (OMWW) was studied by sorption under the conditions of conventional and microwave on previously characterized soils. The sorption process was studied in batch using inorganic materials (soils) in their natural states for sustainable development. The characterizations of the soils have shown variability in the potential of hydrogen (4.6-8.9), in total nitrogen, which is between 0.2 and 2.5%, and in mineral matter, which varies between 6 and 15%. On the other hand, the mineralogical characterization showed that the three adsorbents are composed of several clay and non-clay minerals. The experimental data were analyzed using the reaction and diffusional models. The pseudo-second-order kinetic model provides the best correlation for the three natural adsorbents denoted G (gray), B (black), and R' (red). The sorption models of Langmuir, Freundlich, and Dubinin-Radushkevich were used for the mathematical description of the conventional adsorption equilibrium. The best correlations were obtained with the Langmuir model ($r^2 > 0.95$) on the G and B adsorbents, unlike the Freundlich and Dubinin-Radushkevich models ($r^2 < 0.64$). The adsorbent R' can be represented by the Freundlich model ($r^2 \geq 0.96$) and the Langmuir model ($r^2 > 0.94$). The latter is confirmed by the value of the dimensionless coefficient R_L. The removal rates of TPC were calculated, and the value obtained (71%) shows that the G adsorbent is a good adsorbent. The results are satisfactory and promising.

Keywords: Conventional sorption, microwave irradiation sorption, total phenolic compounds, olive mill wastewater, natural soils, kinetics, and isotherms.

Graphical abstract

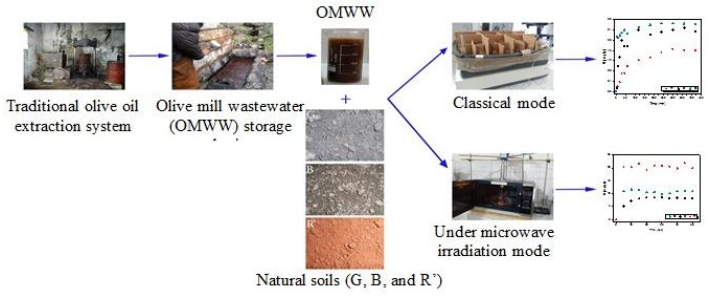

Recommended Citation
Arabi M, Elias A, Ait Younes Y, Kamel Z, Toumert I, Mansouri B. Removal of total phenolic compounds from olive mill wastewater by adsorption on natural soils: characterization of adsorbents, classical and under microwave irradiation kinetics study. *Alger. J. Eng. Technol. 2025, 10(1): 13-34*., http://dx.doi.org/10.57056/ajet.v10i1.189

1. Introduction

Water is essential to life, but it is also very often at the heart of many economic activities. The olive-growing water is industrial wastewater commonly called "vegetable water" and comes from the water during the extraction process of olive oil (the water of the pulp and the added water). The quantity produced depends on the demand for olive oil and its extraction process, which generates effluents at points of concentration of pollutants (polyphenols) not resorbable by the purifying power of the media. They are considered one of the most harmful vegetable discharges by food industries due to the toxicity [1] of their pollutant load for the whole ecosystem (plants, microorganisms, aquatic, and aerial organisms).

Sorption is a very efficient and promising physical separation process used to lower the concentration of toxic organic pollutants from industrial effluents. It is a nonpolluting treatment method, easy to apply, and has already proven itself in polluted water [2, 3].

Most Mediterranean countries are currently concerned by the problem of pollution caused by olive mill wastewater. The treatment of these industrial discharges by adsorption on different solid materials has been the subject of much work on expensive materials such as activated carbon [4], activated clays [5], and inexpensive materials such as banana peel [6], wheat bran [7], etc.

The global objective aimed at this work is summarized in the exploitation of the natural materials in the elimination by conventional adsorption and under microwave irradiation of the polluting organic matter (TPC) contained in the effluents resulting from the olive-oil industry. These adsorbents are very abundant, cheap, and can compete with conventional materials like carbon, silica gel, etc.

2. Materials and Methods

2.1. Materials

The adsorbates used in this work are from the olive industry. They were collected in the region of Tizi-Ouzou in March 2015 from the first storage tank of OMWW according to the standard 5667-3 [8] in dark jerricans of 20 liters in view of their transport to the laboratory for conservation at 4°C.

The adsorbents (soils) used in this work were collected in the vicinity of our vegetation water sampling area (Tizi-Ouzou). They are natural and different between them in color. Drying in the open air was preceded by being ground by a porcelain mortar, sieving at different mesh sizes, and storage at room temperature in plastic boxes before characterizations and sorption experiments.

2.2. Characterization methods

For OMWW, the pH was measured using a WTW multi 340i pH meter according to the NF T 90-008 standard [9]. The electrical conductivity (E.C.), expressed in mS/cm at ambient temperature, was obtained with a digital conductivity meter type K 120 CONSORT according to the French standard NF EN 27888 [10]. The TPC, expressed as gallic acid equivalents per g/L, was determined by the colorimetric method with the Folin-Ciocalteu reagent [11] at the experimental wavelength of 765 nm by a UV-visible spectrometer (T60, PG. Instruments).

Soil pH was determined, according to ISO 10390 [12], in a soil suspension diluted in water at 1:5 (V/V) and using a microprocessor pH meter WTW pH537. For the pH at the zero charge point, its measurement [13] consists of placing in a series of Erlenmeyer flasks 40 mL of the KNO_3 solution (10^{-1} M, Fluka) previously adjusted to the desired pH ranging from 2 to 12 by addition of NaOH or HCl (10^{-1} M), in contact with 0.2 g of soil (Ø < 500 µm). The suspensions must be kept under constant stirring, at room temperature, for 48 h. The final pH is then determined on the supernatant after separation of the two constituents by centrifugation (SIGMA 3-30 KS) at 3000 g and 20 °C for 15 min. The pH_{pzc} is the point of intersection between the curve representing the final pH versus the initial pH and the line pH = initial pH.

The humidity (H) was determined after drying a mass (m) at 105°C for 24 hours. The rate, expressed as a percentage, was calculated according to the formula:

$$H(\%) = \left[\frac{m_0 - m_1}{m_0} \right] \times 100 \qquad (1$$

Where m_0 and m_1 are the mass of the sample before and after drying at 105°C, expressed in grams, respectively.

Soil densities were measured using a helium pycnometer (Micromeritics) connected to a vacuum system and to a helium cylinder via a pressure regulator (0.3-0.5 bar). They are calculated by the formula:

$$d_s = \frac{\rho_s}{\rho_{eau}} = \left[\frac{m_s}{\frac{(m_L - m_i)}{\rho_{eau}}} \right] \quad (2$$

Where ρ_s is the density of the soil, ρ_{water} is the density of the water at the temperature of 4°C, m_s is the mass of the soil (kg), m_L is the mass of the liquid alone (kg), and m_i is the mass of the immersion liquid (kg) in the pycnometer.

The functional groups were identified by Fourier transform infrared spectrometry (NICOLET 380) by preparing pellets of potassium bromide KBr (Merck, MM = 119.01 g/mole) mixed with 1% of soil powder. The identification of the crystallized mineral species of the soils was carried out by X-ray diffraction (XRD), and this was done by comparison with a reference file called JCPDS sheets for "Joint Committee for Powder Diffraction Studies" [14, 15]. The chemical composition of the soils was determined by the wavelength-dispersive X-ray fluorescence technique (WD-XRF). The microstructure of our adsorbents was observed by a scanning electron microscope (SEM) type FEI Quanta 650.

Organic and inorganic matters were determined according to the work of Wang et al. [16]. Organic matter, expressed as a percentage, was calculated according to the formula:

$$MOG(\%) = \left[\frac{m_1 - m_2}{m_1} \right] \times 100 \quad (3$$

Where m_1 and m_2 are the mass of the sample after drying at 105°C and 375°C, expressed in grams, respectively.

On the other hand, the mineral matter was calculated by the formula:

$$MM(\%) = \left[\frac{m_2 - m_3}{m_2} \right] \times 100 \quad (4$$

Where m_2 and m_3 are the mass of the sample after drying at 105°C and 800°C, expressed in grams, respectively.

The loss on ignition was determined after firing our adsorbent at 1000°C for one hour in a muffle furnace. It is expressed as a percentage and evaluated by the following formula:

$$Pf(\%) = \left[\frac{m_1 - m_4}{m_1} \right] \times 100 \quad (5$$

Where m_1 and m_4 are the mass of the sample after drying at 105°C and 1000°C, expressed in grams, respectively.

The cation exchange capacity (CEC.) was measured at pH = 9.0 in a sandwich percolation tube between two layers of 10 g of sand [17].

The specific surface area, also called the mass area, was calculated using the so-called BET (Brunauer-Emmett-Teller) [18] calculation model at nitrogen at 77 K by a Micromeritics ASAP 2010, USA. The particle size distribution was carried out by sieving using a Retsch-type vibrator at a fixed vibration amplitude of 40 for 30 minutes.

2.3. Sorption experimental test

The sorption tests of TPC were studied in static mode (batch). The overall experimental parameters chosen to carry out these tests are time, weight, and particle size of the adsorbent; the dilution factor (TPC concentration); and the pH of the effluent. The latter was adjusted to the required pH using either NaOH (1M) or HCl (1M). At the end of each sorption study, the adsorbents were separated by centrifugation. Three phases are thus obtained: at the bottom, the adsorbent; in the center, the olive oil effluent; and a very light layer of oil on the surface. The content of the TPC was obtained in each case in the medium phase by extrapolation on the calibration plot. The adsorbed quantity (q_e), as well as the removal rate (R %) of the TPC, were calculated before and after adsorption per mass unit of soil and OMWW volume according to the

equations, respectively:

$$q_e = \left[\frac{C_0 - C_e}{w}\right] \times V \quad (6$$

$$R(\%) = \left[\frac{C_0 - C_t}{C_0}\right] \times 100 \quad (7$$

Where C_0, C_e, and C_t are, respectively, the initial, the equilibrium, and at the time (t), the concentrations of the TPC in the solution during the adsorption process (g/L). V is the volume of the solution (L), and w is the weight of the sorbent (g).

In classical mode, the sorption test experiment was carried out at room temperature and protected from light. For this, a volume of non-delipidated oleic effluents was brought into contact with a known weight of each soil separately in open reactors (50 mL Erlenmeyer flask). The suspensions were shaken by a multi-station system (Gesellschaft für Labortechnik mbH, 3015). For each experiment, a control pot was produced under the same conditions without the solid. On the other hand, under irradiation, the sorption tests were carried out in a modified domestic microwave oven of the SAMSUNG brand in beakers (Ø = 4.5 cm; length = 6.8 cm). Once the contact between the adsorbent and the adsorbate was made, the reactor was placed inside the microwave oven. The dispersion was ensured using a glass rod previously installed in the arm of a mechanical stirrer of the IKA RW 20n brand. The microwave irradiation was programmed for a time t with steps equal to 5 seconds. The parameters that were studied are:

- The contact time between the adsorbent (soils) and the adsorbate (TPC), which is an important parameter generally influencing the sorption process. It allows us to determine the removal rate of TPC and consequently to evaluate the efficiency of the adsorbent. The sorption conditions applied in the conventional method were 2 g of the soil of particle size equal to 400 µm and an initial concentration of TPC in OMWW equal to 2.910 g/L. The time was varied from 5 to 420 minutes, and the stirring speed was set at 250 rpm. The experimental protocol, which was carried out in a 50 mL capacity reactor, is as follows: 20 mL of diluted olive mill wastewater ([TPC] = 0.728 g/L) with deionized water is added to 2 g of the soil of particle size equal to 400 µm. The solids loading in the liquid is 100 g/L. Several flasks were thus prepared, and the suspensions were shaken at room temperature (20 ± 5°C) at the stirring speed of 250 rpm at the natural pH of the effluent and soil for varying times ranging from 5 to 420 minutes (contact time per flask). After shaking, the suspension was thus centrifuged and ready for the determination of the TPC.
- Mass on TPC sorption capacity: This test was studied in the range 0.5–3.5 g with 0.5 g increments for 24 h to ensure equilibrium.
- The particle size of the adsorbent on the sorption of TPC was studied, ranging from 40 to 400 µm for the three adsorbents, taking into consideration the mass of the adsorbent previously optimized.
- The pH on TPC sorption by natural soils was also studied using the parameters optimized in previous experiments, such as mass and particle size. The pH values explored ranged from 3 to 10.
- The study of the effect of the content of TPC on the sorption capacity consists of following the influence of the initial concentration of the solute on the quantity adsorbed by the adsorbent ranging from the content of 5 mg/L to 189 mg/L. The mass, the particle size, and the pH used are those optimized previously.
- The effect of microwave irradiation was also studied. For this, the conditions were set at a weight equal to 0.5 g of soil at 40 µm, a power of 180 W, a TPC concentration equal to 663 mg/L, and variable times ranging from 5 up to 50 seconds with steps of 5 seconds repeated several times to avoid boiling (one contact time per flask). The stirring speed was set at 250 rpm.

2.4. Kinetic studies

The adsorption kinetics allows estimating the quantity of pollutants adsorbed as a function of time. It provides information on the adsorption mechanism and the mode of transfer of solutes from the liquid phase to the solid phase. At equilibrium, the adsorption kinetics of a material can be modeled. For this purpose, the literature reports some models that can register as follows:

Pseudo-first order model [19]

$$Ln(q_e - q_t) = Lnq_e - k_1 \times t \quad (8$$

Pseudo-second order model [20, 21]

$$\left(\frac{t}{q_t}\right) = \left(\frac{1}{k_2 \times q_e^2}\right) + \left(\frac{1}{q_e}\right) \times t \quad (9$$

Intra-particle-scattering model [22]

$$q_t = k_{\text{int}} \times t^{1/2} + Z' \quad (10$$

Extern scattering model [5, 23]

$$Ln\left[1 - \left(\frac{q_t}{q_e}\right)\right] = -0.497 - k_b \times t \quad (11$$

Where k_1 (unit of time^{-1}), k_2 (g/mg unit of time), k_{int} (mg/g unit of time^{0,5}), and k_b (unit of time^{-1}) are the rate constants for the model: pseudo-first-order, pseudo-second-order, intra-particle scattering, and external scattering. q_e and q_t (mg/g) are the amounts of solute absorbed per unit adsorbent at equilibrium and at time t, respectively. *Z'* is the parameter that reflects the deviation of the adsorption process from the intra-particle scattering mechanism.

2.5. Isotherm studies

The adsorption isotherms of TPC at the equilibrium of the solid-liquid system were determined using the Langmuir, Freundlich, and Dubinin-Radushkevich (D-R) models.

The linearization of the equation of the Langmuir model is given by the relation

$$\frac{C_e}{Q_{eq}} = \frac{1}{Q_{\max} \times K_L} + \frac{1}{Q_{\max}} \times C_e \quad (12$$

Where Q_e and Q_{max} (mg/L) are the adsorption capacity at equilibrium and maximum of the adsorbent, respectively. C_e is the equilibrium concentration of the TPC in the liquid phase (mg/L), and K_L is the Langmuir equilibrium constant characteristic of the adsorbent (L/mg).

The plot (C_e/Q_e) versus C_e gives a line with slope ($1/Q_{max}$) and intercept ($1/Q_{max}$. K_L). The essential characteristics of the Langmuir isotherm can be expressed by a dimensionless constant called the separation factor or equilibrium parameter "R_L" [24].

$$R_L = \frac{1}{1 + (K_L \times C_e)} \quad (13$$

The value of this factor indicates the isotherm type: unfavorable if $R_L > 1$, linear if $R_L = 1$, favorable if $0 < R_L < 1$, or irreversible if $R_L = 0$.

The linear form of the Freundlich model is given by the relation

$$LnQ_e = LnK_F + \left(\frac{1}{n}\right) \times LnC_e \quad (14$$

This equation is that of a straight line with slope 1/*n* and intercepts *ln* K_F. In general, adsorption is favorable when (1/*n*) is between 0 and 1 [25].

Where Q_e and Q_{max} (mg/L) are the adsorption capacity at equilibrium and maximum of the adsorbent, respectively. C_e is the equilibrium concentration of TPC in the liquid phase (mg/L). K_f and 1/*n* are the Freundlich constants.

For the third model used, the linear form of its equation is given by the relation

$$Lnq_e = Lnq_{\max} - \beta' \times R^2 \times T^2 \left[Ln\left(1 + \frac{1}{C_e}\right)\right]^2 \quad (15$$

Where q_{max} is the theoretical saturation capacity (mg/g), *β'* is a constant related to the adsorption energy (mol/kJ)^2, *R* is the perfect gas constant (8.314 10^{-3} kJ/mol K), *T* is the solution temperature (K), and C_e is the equilibrium concentration of TPC in the liquid (mg/L).

The constant *β'* is relayed to the free energy E_D by the relation

$$E_D = \frac{1}{(2 \times \beta')^{1/2}} \quad (16$$

The "E_D" value allows us to determine the nature of the physical or chemical adsorption process. According to the literature [26]: if E_D < 8 kJ/mol, the adsorption process is physical; if E_D is between 8 and 16 kJ/mol, the adsorption is an ion exchange process; if E_D > 16 kJ/mol, the process is dominated by intra-particle diffusion (chemical).

3. Results and Discussion

3.1. Olive vegetation water characterization

The main characteristics of the olive vegetation water used to conduct the adsorption tests are summarized in Table 1. They show that the olive oil discharges are acidic and rich in organic pollutant matter.

Table 1. Main characteristics of olive mill vegetation water.

Parameter	**pH**	**E.C. (mS/cm)**	**TPC (g/L)**
Measured value	4.55	8.61	2.910 ± 0.014

E.C.: electrical conductivity; TPC: total phenolic compounds

3.2. Adsorbent properties

The main chemical properties and characteristic composition of the soils studied are given in Table 2. They show that the B soil is acidic (pH = 4.6), which is due to the presence of humic and fulvic substances and the oxidation of inorganic compounds such as iron sulfide [27, 28]. The other two soils (G and R) have an alkaline pH of 8.9 and 8.4, respectively. This may be due to the presence of carbonates [27, 28]. Adsorbent B is characterized by higher total nitrogen content (2.5%) compared to 0.85% for adsorbent G and 0.2% for adsorbent soil R'.

Table 2. Physico-chemical characterization of the studied adsorbents.

Adsorbent → / Parameter ↓	G	B	R’
pH (H_2O)	8.9	4.6	8.4
E.C. (dS/m)	0.13	0.04	0.06
d^{20} (g/cm^3)	3.39	2.83	3.14
H (%)	4.25	3.95	4.90
OM (%)	1.822 ± 0.429	2.122 ± 0.113	2.383 ± 0.383
OC (%)	0.911 ± 0.214	1.061 ± 0.57	1.191 ± 0.192
MM (%)	15.159 ± 0.254	10.918 ± 0.371	5.860 ± 0.182
MC (%)	4.137 ± 0.69	2.980 ± 0.101	1.599 ± 0.50
TC (%)	5.048 ± 0.279	4.041 ± 0.151	2.791 ± 0.219
TN (%)	0.85	2.50	0.20
PI (%)	16.547 ± 0.75	13.145 ± 0.675	7.631 ± 0.78
Ss (m^2/g)	33.181	24.234	37.800
CEC. ($mg/10^2.g$)	24.54	22.77	24.32
Total limestone (%)	25.78	1.87	1.87

E.C.: electrical conductivity; d: measured density at 20°C; H: humidity; TN: total nitrogen; OM: organic matter; OC: organic carbon; MM: minerals matter; MC: mineral carbon; TC: total carbon; Pl: fire loss; Ss: specific surface; CEC.: cation exchange capacity.

Mineral matter is present in all three adsorbents. The adsorbent G has the highest content of mineral matter (15%), inorganic carbon (4%), and especially limestone (26%). This last parameter may be the reason for the alkaline character of this soil. The greatest value of a loss on ignition is also recorded for the adsorbent G (17%) compared to 13% for the one noted B and 8% for the adsorbent R’. These values are considered low for all soils and indicate that they are low in volatile species. The values of the other characteristics are quite similar for all the samples, notably the cation exchange capacity (23-25 mg/10².g), the moisture content (4-5%), the organic matter content (1.82-2.38%), and the organic carbon content (0.91-1.19%). The specific surface area is variable in the three soils (24-38 m²/g) and remains very low compared to that of clay (700-800 m²/g) [29].

The particle size distribution (Fig. 1) shows that the soils are characterized by a high percentage of the greater fraction of more than 40 µm (> 97%) for all the soils studied. The lutite fraction (< 40 µm) is also present; it respectively represents 0.42, 2.09, and 2.31% for R’, B, and G soils.

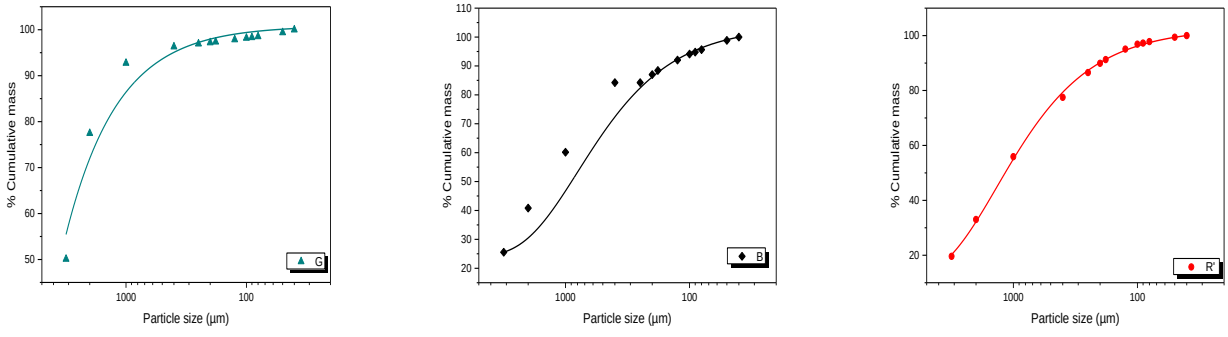

Fig 1. Particle size distribution of raw soils determined by sieving.

The physical and chemical characteristics of the surface of these adsorbents are different. This is shown by the pH values at the zero point charge (pH_{pzc}) of the three adsorbents B, R', and G, which are respectively 4.11, 6.39, and 8.17 (Fig. 2).

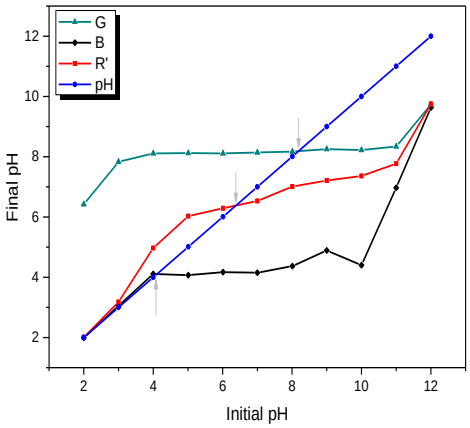

Fig 2. Curves: final pH = f (initial pH), the line: final pH = initial pH, and the points pH_{pzc} of the three adsorbents.

For the mineralogical composition of each adsorbent in the raw state (Fig. 3), we can say that it is complex, varied, and specific.

According to the JCPDS [14] sheets, it corresponds to different minerals constituting the three adsorbents (Table 3). Each adsorbent is composed of several clay minerals and various other non-clay minerals. Some constituents are found in all the studied adsorbents, such as quartz and muscovite. Kaolinite is also present in two soil samples, G and R'.

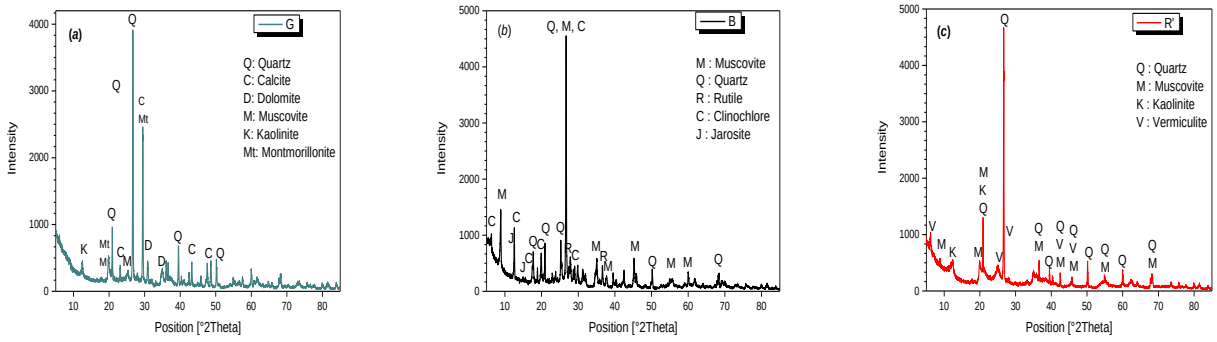

Fig3 X-ray diffractograms of raw soils

Table 3: Mineralogical composition of the soils according to X-ray diffractograms.

Soils	Clay mineral composition/formulas	Various mineral compositions/formulas
G	Muscovite ($KAl_2(AlSi_3O_{10})(OH)_2$), Montmorillonite ($Si_4O_{10}Al_{5/3}Mg_{1/3}Na_{1/3}(OH)_2$), Kaolinite ($Al_2Si_2O_5(OH)_4$))	Quartz (SiO_2), Anatase (TiO_2), Calcite ($CaCO_3$), Dolomite ($Ca\ Mg(CO_3)_2$)
B	Muscovite, Clinochlor ($Al_2Mg_5Si_3O_{10}(OH)_8$)	Quartz, Rutile (TiO_2), Jarosite ($K(Fe_3(SO_4)_2(OH)_6$)
R'	Muscovite, Kaolinite, Vermiculite $(Mg, Ca)_{0,7}(Mg, Fe, Al)_6\ (Al, Si)_8O_{22}(OH)_4\ 8H_2O$)	Quartz

The metallic element composition of the three soils was determined by the wavelength dispersive x-ray fluorescence (WD-XRF) technique. It is expressed in oxide equivalent and presented in mass percentages in Table 4. The silica (SiO_2) and alumina (Al_2O_3) percentages are the highest in all soils. These results are in agreement with those of the XRD, which revealed the richness of its soils in clay minerals (aluminosilicates) and quartz. These soils are also rich in iron; the high value in adsorbent R' may explain its red color. The high calcium oxide content in soil G also confirms the results of the XRD, which revealed the presence of calcite only in this sample. The metals Mg, Mn, Fe, Al, and Si generally constitute the tetrahedral and octahedral layers of clays. Sodium, potassium, and calcium are also known as exchangeable cations incorporated in the interfoliar space of clay sheets. The results of this analysis conform to those of the XRD, confirming the composition of clays and quartz in the studied raw soils.

Table 4: Soils metals oxides composition (mass %).

Adsorbent → / **Parameter ↓**	**G**	**B**	**R'**
SiO_2	42.21 ± 0.10	45.15 ± 0.10	44.84 ± 0.10
Al_2O_3	14.57 ± 0.10	23.48 ± 0.10	27.44 ± 0.10
Fe_2O_3	5.41 ± 0.07	8.14 ± 0.08	12.34 ± 0.10
CaO	12.42 ± 0.10	0.12 ± 0.01	0.45 ± 0.02
MgO	3.18 ± 0.05	2.48 ± 0.05	1.96 ± 0.04
K_2O	2.33 ± 0.04	4.76 ± 0.06	1.34 ± 0.03
Na_2O	0.51 ± 0.02	0.63 ± 0.02	0.29 ± 0.02
MnO	0.040 ± 0.006	0.020 ± 0.004	0.11 ± 0.01
TiO_2	0.66 ± 0.02	1.24 ± 0.03	1.18 ± 0.03
P_2O_5	0.19 ± 0.01	0.31 ± 0.02	0.10 ± 0.01
SO_3	0.56 ± 0.02	1.64 ± 0.04	0.05 ± 0.06
Total	82.08	87.97	90.1

The IRTF spectra of the G, B, and R' adsorbents shown in Fig. 4 reveal the vibration bands of the bonds constituting the minerals that make up the studied soils.

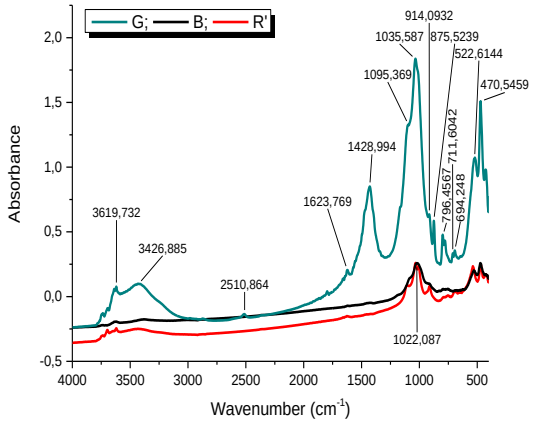

Fig 4. IRTF spectra of soils G, B, and R'.

The main vibrational bands of the bands [30-36], which characterize the minerals present in the studied soils, are grouped in Table 5. These results show that the observed vibrational bands correspond well to those of the aluminosilicate minerals that generally compose clays. These bands are Si-O, O-H, and Al-O-H, which are found, notably, in montmorillonite, muscovite, kaolinite, vermiculite, clinochlore, and quartz. This further confirms that these minerals make up the studied soils and thus join with the results revealed by XRD and WD-XRF.

Table 5: IRTF spectra interpretation of the studied soils.

Soils and wave numbers corresponding to the vibration bands (cm^{-1})			**Vibration type**
G	**B**	**R'**	
3619.732	*	3619.732	Elongation of structural O-H band
3426.885	*	3426.885	Elongation of O-H band in hygroscopic water
1623.769	*	*	Deformation of O-H band of water molecules
1428.994	*	*	Vibration C-O of the calcite
1095.369; 1035.587	1095.369; 1022.087	1095.369; 1022.087	Si-O valence vibration in clays
914.09	914.02	914.09	AlAlOH deformation
875.5	*	*	The vibration of the C-O band of calcite
796.457	*	*	The vibration of the Si-O band in quartz
711.604	*	*	
694.248	*	*	The vibration of OH deformation
522.614	522.614	522.614	Vibration of Si-O
470.545	470.546	470.546	Si-O band of Quartz

The sign * indicates that the band is not observed in the IR spectrum of the corresponding soil.

The scanning electron microscope observations show that the G and B adsorbents appear to have a more porous surface than the third adsorbent, R', which appears with a rough image (Fig. 5). The grain size ranges between 0.89 and 5.559 µm.

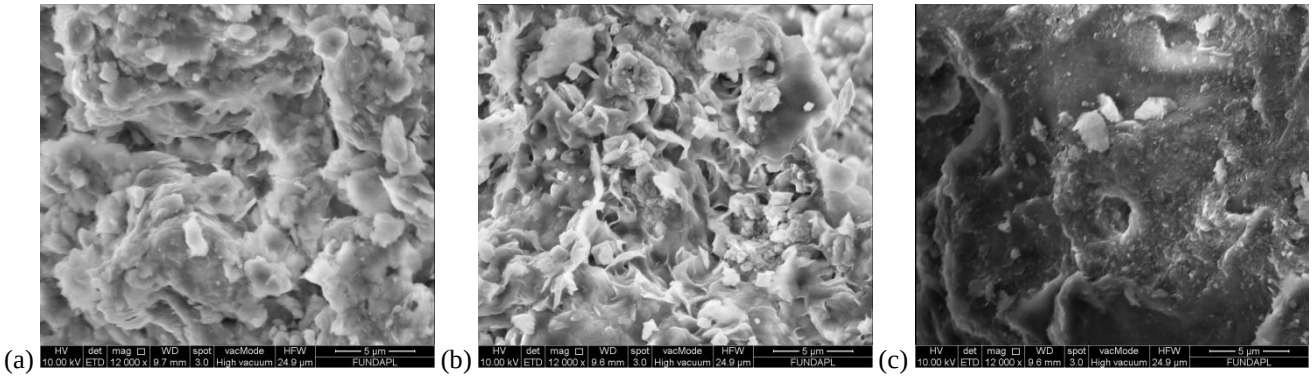

Fig 5. SEM micrographs of soils **(a)** G, **(b)** B, and **(c)** R'.

The EDX analysis perfectly confirms the results obtained by the mineralogical and chemical analyses. It clearly shows the intensity of the calcium peak, characteristic of carbonates, which appears very high only in G soil (Fig. 6 a).

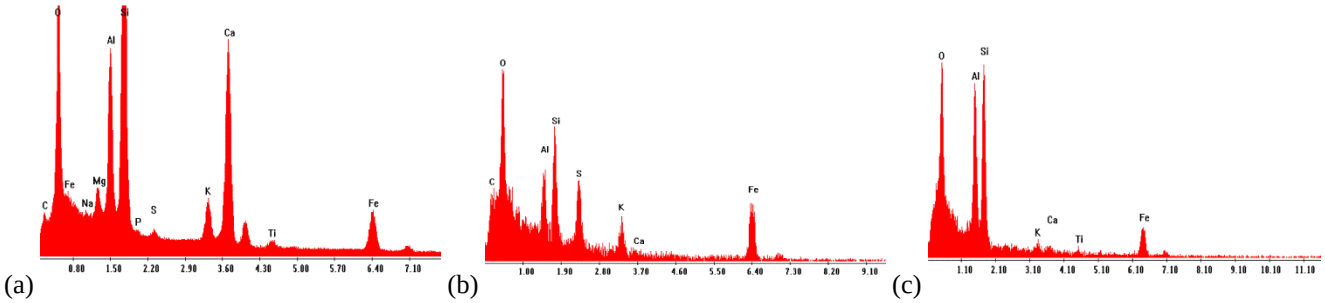

Fig 6. EDX analysis of soils (a) G, (b) B, and (c) R'.

The high calcium content in the G soil is also confirmed by the results of other analyses, notably XRD and X-ray fluorescence. The EDAX spectra also reveal the presence of silicates, characteristic of quartz and clays that compose the three soils. It is important to note, according to the EDAX spectra, that the chemical composition of the soils is predominantly by the elements Si, Al, and Fe, with the addition of the element S for the B soil and Ca, Mg for the G soil, which contains calcite and dolomite, according to the XRD analysis. The EDAX spectra also reveal the presence of other peaks of low intensity, reflecting the presence of other elements with lower contents, such as phosphorus, sulfur, and titanium in G soil; and calcium in B soil; potassium, calcium, and titanium in R' soil.

Thermal degradation profiles obtained from differential thermal analysis (DTG) of the three soils (G, B, and R') are shown in Fig. 7. Several endothermic peaks (DT < 0) appear between 73 and 377.5°C but the most intense is between 73-75°C, accompanied by mass losses of 0.75, 0.60, and 0.85% for G, B, and R', respectively. The latter is generally attributed to the dehydration of water initially adsorbed on the surface and in the pores of the different minerals constituting the soils. Beyond 200°C, mass losses may be due to the transformations of humic substances in the soils, as in the case of adsorbent B at 377.5°C. Other endothermic peaks are observed for the three adsorbents, but the most intense is that of adsorbent G, which is at 755.47°C. It is associated with almost all of the mass loss (14.87%) of this sample, probably corresponding to the decomposition of calcite and dolomite, which are particular constituents of the G soil.

The exothermic phenomenon (DT > 0) is also observed for the three soils at 890.8 (G), 819.8 (B), and 821.5°C (R'), which can be attributed to the structural reorganization of clay minerals.

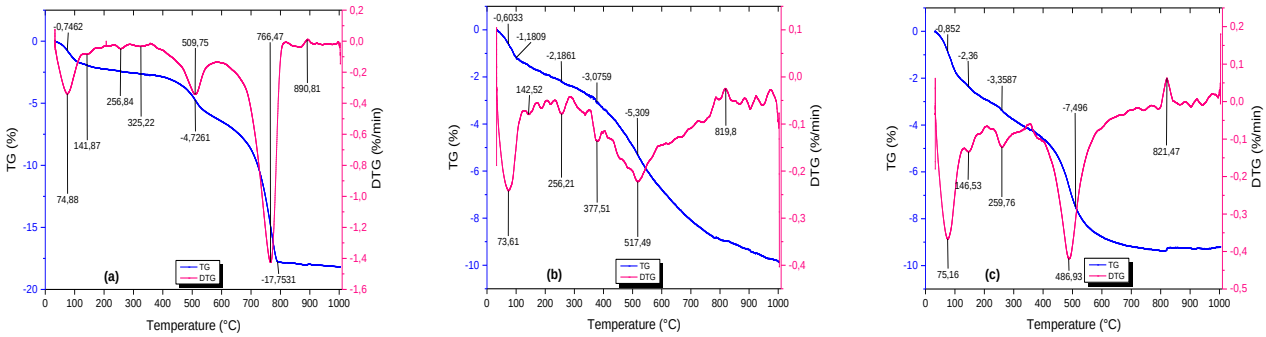

Fig 7. TG-DTG spectra of soils (a) G, (b) B, and (c) R'.

3.3. Sorption studies

- Effect of contact time: These curves present two phases and show that the time to almost reach adsorption equilibrium is about 2 h for the G soil and 4 h for the B and R' soils (Fig 8). The first phase, during which adsorption of almost all of TPC occurs, is characterized by a relatively short duration (1 h) and a rapid adsorption speed. In the second phase, which ends in equilibrium, the adsorption speed and the adsorbed amount are low. Adsorption is faster in the case of G soil, and its adsorption capacity at equilibrium is the highest (70%); it is double that of R' soil (46%). This can be explained by the low porosity of the R' soil (see SEM image). Comparing our results with those of the literature, we deduce that the adsorption process of TPC on our adsorbents is slow too and agrees with the results (2-12 hours) of many studies [5, 6, 37-43], such as those carried out on clay minerals (bentonite) from Maghnia (Algeria). However, according to some studies, the kinetics can be much faster in the cases of some activated adsorbents, such as the adsorption of phenol to activated carbon [44] and on some activated clays [45]. The contact time chosen for the remainder of our studies is 24 hours to ensure that equilibrium is reached for the three adsorbents G, B, and R'.

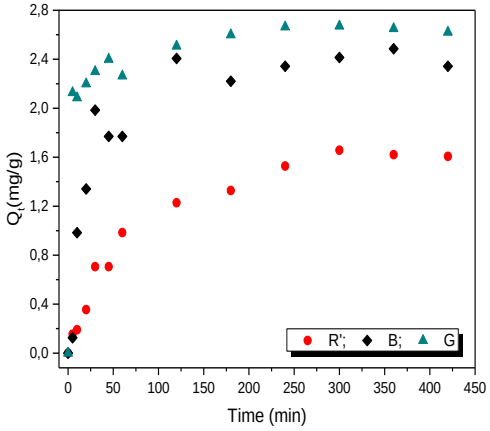

Fig 8. Effect of contact time on the adsorption capacity of TPC (m = 2 g; Ø = 400 µm; $pH_{effluent}$ = 4.55; [TPC] = 728 mg/L; stirring speed = 250 rpm; v = 20 mL; T = 25 °C).

- Effects of amount on the adsorption capacity of TPC: The results show that during the removal of TPC by adsorption on natural soils, the removal rate increases with the weight of adsorbent used (Fig 9). It reaches 69, 70, and 73%, respectively, on B, G, and R' soils. According to the work of Garg et al. [46], the increase in percent adsorption with soil mass may be due to the increase in adsorbent surface area and adsorption sites [47, 48]. The best removal rate is obtained for weights ranging from 3 to 4 g for all soils.

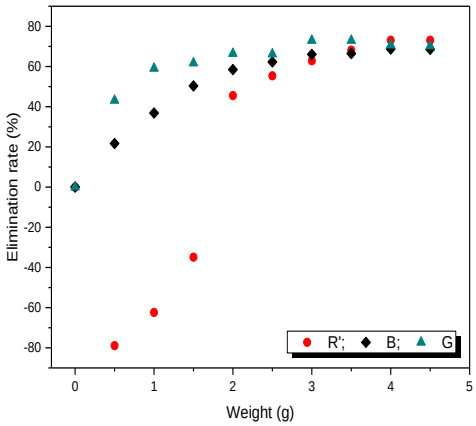

Fig 9. TPC removal rate as a function of the mass of the adsorbent (Ø = 400 µm; $pH_{effluent}$ = 4.55; [TPC] = 728 mg/L; stirring speed = 250 rpm; v = 20 mL; T = 25 °C; t = 24 h).

- Effects of the soil particle size of the adsorbent on the adsorption of TPC: The results show that the increase of the particle size decreases the adsorption capacity of the TPC (Fig 10) due to the decrease in the specific surface, thus decreasing the adsorption capacity. The best removal rate is obtained for the fine fractions (Ø = 40 µm).

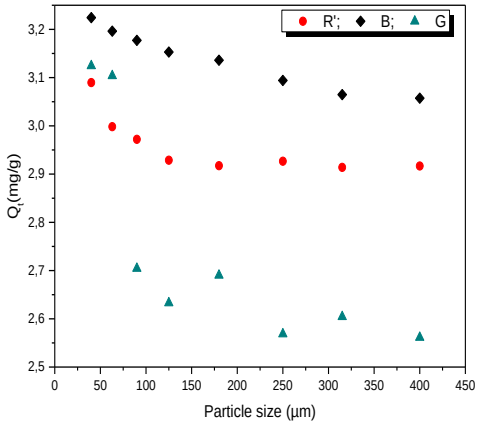

Fig 10. Influence of particle size on the adsorption capacity of TPC ($pH_{effluent}$ = 4.55; [TPC] = 728 mg/L; stirring speed = 250 rpm; v = 20 mL; T = 25 °C; t = 24 h; m = 3.5 g).

- Effects of effluent pH on adsorption capacity of TPC: The effect of pH on the adsorption capacity of TPC from effluent by natural adsorbents (G, B, and R') shows that the adsorption is largely affected by the pH of the solution (Fig 11). The adsorption capacity of TPC in an acidic solution is important for all soils. It is max around the pH of the effluent (4.55) for B (89%) and G (71%) adsorbents. For the adsorbent R', the adsorption capacity (78%) is almost constant over the whole pH range. Comparable results were also found in some studies on phenol adsorption, such as those published by Djebbar et al. [40] on clays and by Datta et al. [49] on an ion exchange resin.

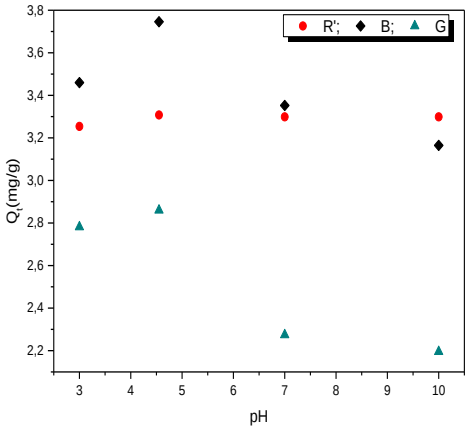

Fig 11. Influence of pH on the adsorption capacity of TPC ([TPC] = 728 mg/L; stirring speed = 250 rpm; v = 20 mL; T = 25 °C; t = 24 h; m = 3.5g; Ø = 40 µm).

- Effect of microwave irradiation: The temperature at the stop of the reaction of microwave irradiation for the studied adsorbents is variable (Fig 12). It varies between 37°C (B) and 33°C (G).

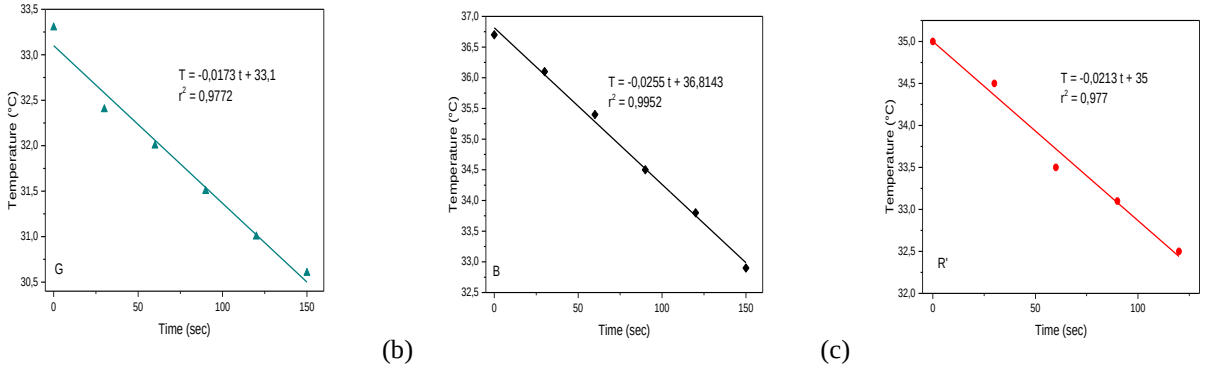

(a) (b) (c)

Fig 12. Temperature variation after microwave irradiation of natural soils (a) G, (b) B, and (c) R' (stirring speed = 250 rpm; power = 180 W; m = 0.5 g; Ø = 180 µm; t= 60 sec with steps of 5 sec; [TPC] = 663 mg/L; v = 20 mL at pH = 4.55).

The effect of contact time under irradiation microwave is represented by the curves of Fig 13. The latter shows that the adsorption rate of TPC by the three adsorbents (G, B, and R') evolves rapidly until reaching saturation. We can say that microwave irradiations generate a very fast rotation of the molecules. Thus, it creates instantaneous heating of the medium and a movement of additional shock between the molecules, which increases the probability of interaction and the speed of reactions. The retention by the adsorbent R' is faster than in the case of the other adsorbents G and B. This difference in adsorption retention comes from the specific surface of relatively higher soil R' (38 m^2/g) than those of other soils G (33 m^2/g) and B (24 m^2/g). Indeed, according to the literature, microwave irradiations accelerate reaction speeds and increase adsorption capacity [50] while preserving the pore structure and active adsorption sites capacity [51].

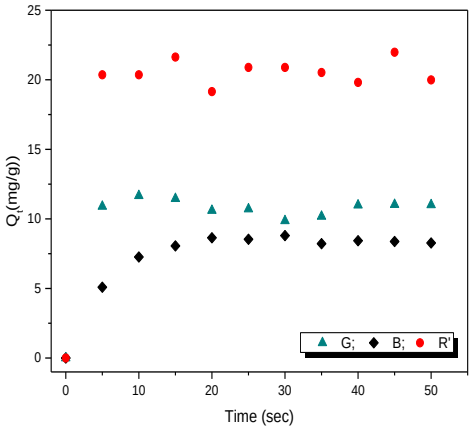

Fig 13. Influence of contact time on the adsorption of TPC under microwave irradiation (stirring speed = 250 rpm; power = 180 W; m = 0.5 g; Ø = 40 µm; [TPC] = 663 mg/L; v = 20 mL; pH = 4.55; t = 50 sec with steps of 5 sec).

Comparing our results with similar work in the literature (Table 6, Fig 8, Fig 13: effect of contact time on adsorption of TPC), we note that our soil samples are effective in removing the total phenolic compounds in aqueous solutions under the effect of microwave irradiation. Finally, the use of microwave activation reduced the time required to reach equilibrium.

Table 6. Comparison of the amount of phenol adsorbed by different adsorbents.

Author's	**Absorbents**		**Maximum sorption capacity (mg/g)**
Arellano-Cárdenas et al. [52]	Porous clay heterostructure		14.5
Chen et al. [53]	Solidified clay		8.4
Chaudhary and Balomajumder [39]	Fly ash impregnated with aluminum		12.67
This work	Natural soil G	Conventional sorption	2.67
		Sorption under microwave irradiation	10.63
	Natural soil B	Conventional sorption	2.49
		Sorption under microwave irradiation	8.82
	Natural soil R'	Conventional sorption	1.66
		Sorption under microwave irradiation	19.76

3.4. Sorption kinetics

The plots of the TPC sorption kinetics (Fig 14 and Fig 15) show that the pseudo-second-order model is appropriate to describe the TPC adsorption reactions by the three soils (G, B, and R') for the two processes because the determination coefficients are much closer to unity, so this model describes the empirical results well.

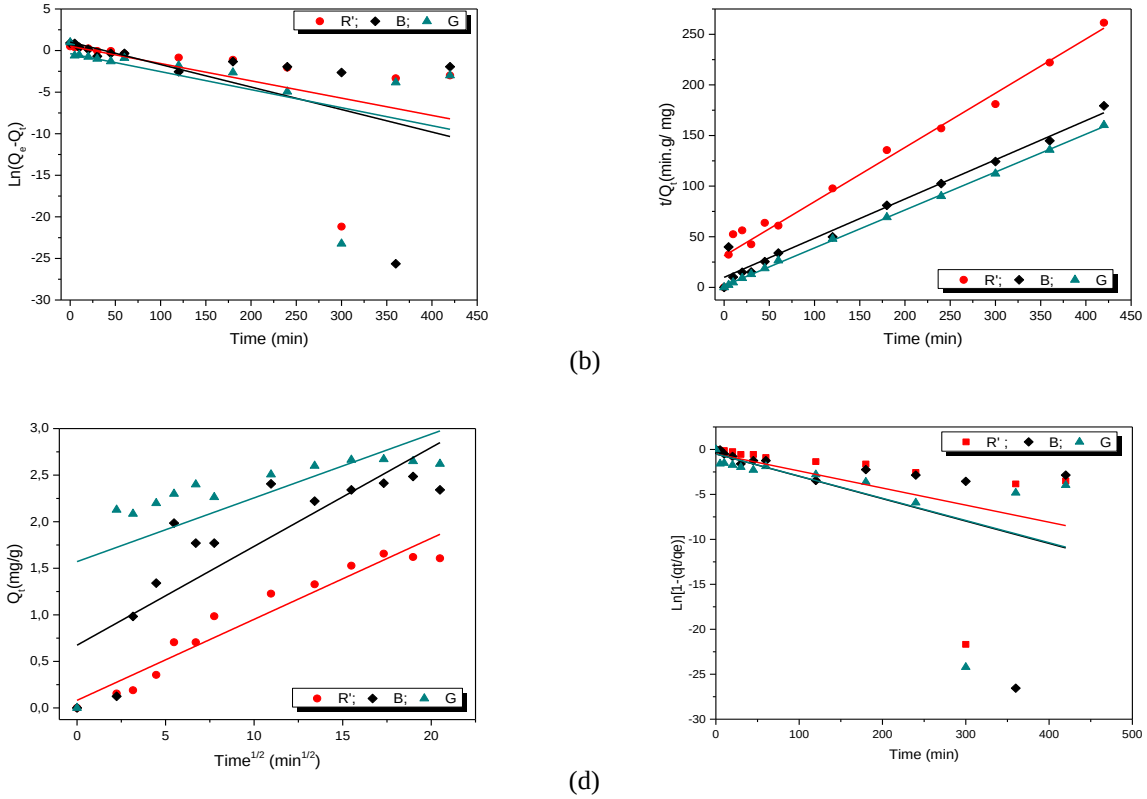

(a) (b)

(c) (d)

Fig 14. Kinetic linearization of conventional adsorption of TPC on natural soils (a) pseudo-first-order, (b) pseudo-second-order, (c) intra-particle diffusion, and (d) external diffusion.

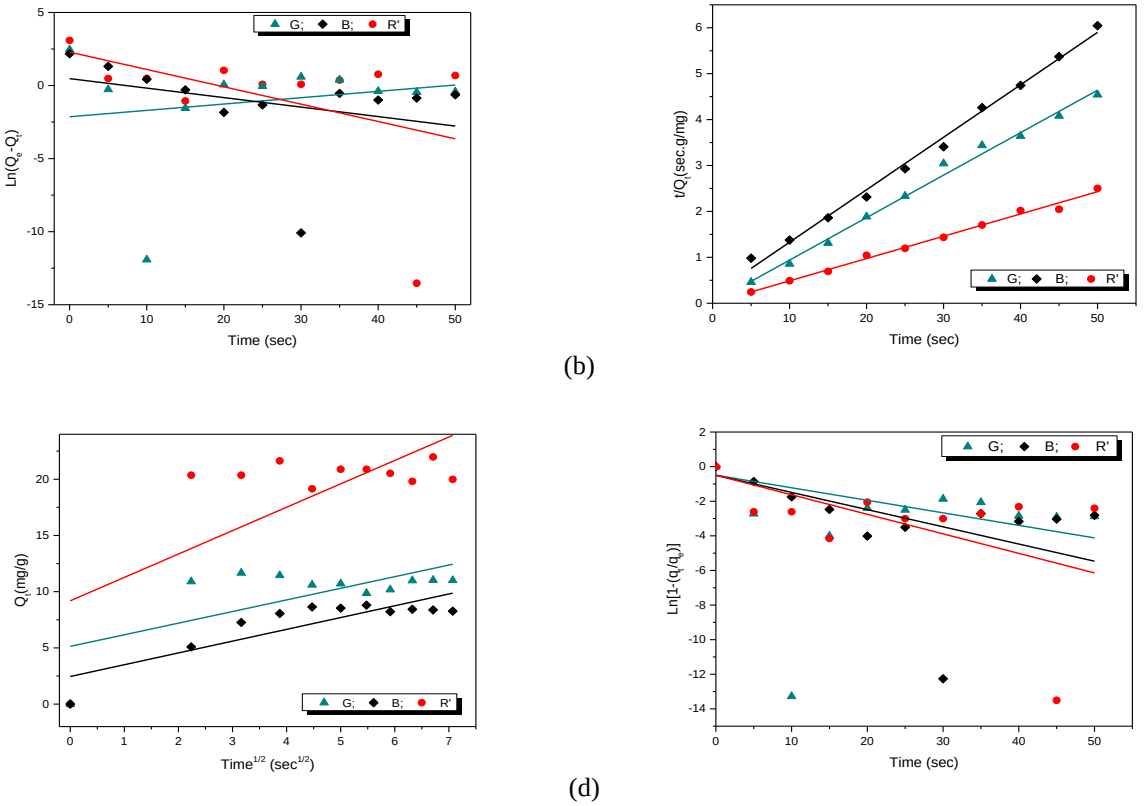

(a) (b)

(c) (d)

Fig 15. Kinetic linearization of adsorption under microwave activation of TPC on natural soils (a) pseudo-first-order, (b) pseudo-second-order, (c) intra-particle diffusion, and (d) external diffusion.

The kinetic parameters (k_2, q_e, and r^2) deduced from the applied kinetic models are summarized in Table 7. The determination coefficients r^2 obtained for the pseudo-second-order model are for the conventional adsorption equal in decreasing order to 1.000, 0.975, and 0.971 for G, R', and B adsorbents, respectively, and equal to 0.99 for adsorption under microwave irradiation.

Table 7: Calculated kinetic parameters of the studied models for the sorption of TPC in OMWW on the three adsorbents.

	Adsorbents →	**G**		**B**		**R'**	
	Sorption process →	**Conv.**	**µ.wave**	**Conv.**	**µ.wave**	**Conv.**	**µ.wave**
Models ↓	**Parameters ↓**						
Pseudo-first-order	k_1 **(min^{-1})**	0.022		0.027		0.021	
	k_1 **(sec^{-1})**		0.044		0.065		0.119
	Q_{max} **(mg/g)**	0.693	0.118	2.793	1.605	1.684	9.836
	r^2	0.201	-0.070	0.264	0.016	0.214	0.114
Pseudo-second-order	k_2 **(g/mg.min)**	0.211		1.479		8.923	
	k_2 **(g/mg.sec)**		12.423 10^{-5}		244.344 10^{-5}		0.766 10^{-5}
	q_e **(mg/g)**	2.669	10.807	2.583	8.752	1.867	20.602
	r^2	1.000	0.991	0.971	0.993	0.975	0.991
Intra-particle scattering	k_{int} **(mg/g.min^{0,5})**	0.068		0.106		0.087	
	k_{int} **(mg/g.sec^{0,5})**		1.033		1.049		2.081
	Z'	1.571	5.135	0.674	2.455	0.082	9.187
	r^2	0.389	0.383	0.689	0.701	0.934	0.450
External scattering	k_b **(min^{-1})**	0.025		0.025		0.019	
	k_b **(sec^{-1})**		0.072		0.099		0.113
	r^2	0.475	0.283	0.429	0.534	0.377	0.585

Conv.: Conventional; µ.wave: microwave

The values of adsorbed quantities Q_e calculated by this model are very close to the experimental values for the two sorption processes: conventional and under microwave activation (Table 8). This shows that the adsorption kinetics are perfectly described by the pseudo-second-order kinetic model for the three adsorbents chosen to conduct this study.

Table 8. Sorption quantities of TPC.

	Q_e **(mg/g)**					
	Conventional sorption			**Under microwave activation sorption**		
Soils (adsorbent)	**G**	**B**	**R'**	**G**	**B**	**R'**
Experimental values	2.671	2.485	1.657	11.689	8.820	21.979
Measured values	2.669	2.583	1.867	10.807	8.752	20.602

Similar results were observed for the adsorption of phenolic compounds by banana peel, wheat bran, and activated carbon [4, 7, 43]. Also, Silva et al. [54] showed that the sorption of aromatic compounds on clay supports obeys the pseudo-second-order kinetic model.

According to Ho et al. [55], the adsorption is a chemisorption type with the involvement of valence forces by electrons sharing or exchanging between the adsorbent and the adsorbate.

3.5. Sorption isotherm

The adsorption capacities of TPC increase with the initial concentration of the latter until saturation of the adsorption sites, indicated by a plateau. The obtained plots are illustrated in Fig 16. The maximum quantity adsorbed (Q_{max}) is about 0.1 mg of TPC/g of adsorbent, or exactly 0.098, 0.103, and 0.108 mg/g for B, G, and R' adsorbents, respectively. These quantities correspond to equilibrium concentrations of TPC equal to 22.5 mg/L for G and B adsorbents and 20 mg/L for R'

adsorbent. These results show that the equilibrium concentrations of TPC in the aqueous phase and the three adsorbents are near.

The sorption isotherms of TPC on the three natural soils present a classical L-type appearance, subgroup 1 for G, B adsorbents, and subgroup 2 for R' adsorbent.

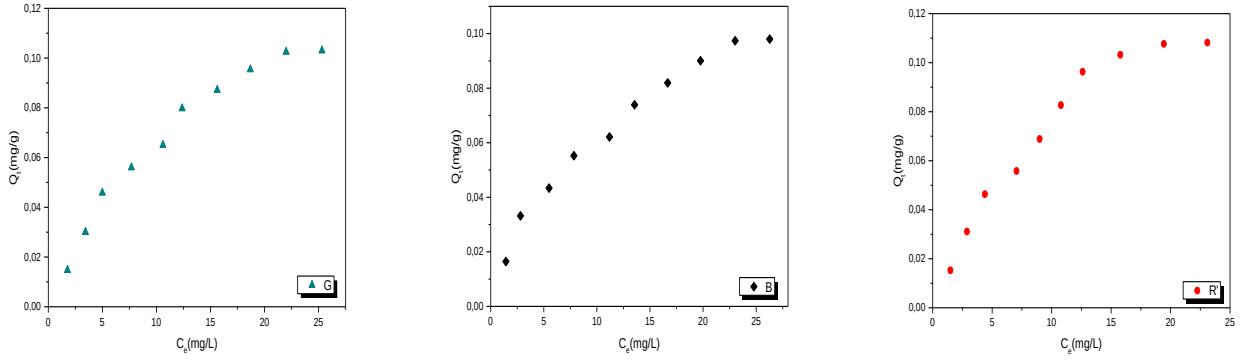

Fig 16. Influence of the initial TPC concentration (stirring speed = 250 rpm; v = 20 mL; T = 25 °C; t = 24 h; m = 3.5 g; Ø = 40 µm; $pH_{effluent}$ = 4.55).

The models of these adsorption isotherms, illustrated in their linear forms, are illustrated by the plots in Fig 17, Fig 18, and Fig 19. The parameters obtained from these models (K_F, $1/n$, Q_{max}, K_L, β, E_D, and r^2) for the conventional adsorption of TPC on the three natural adsorbents are determined graphically and listed in Table 9.

According to the values of the determination coefficient r^2, it can be seen that the Langmuir model gives a good representation of the adsorption of TPC: 0.957 (G), 0.972 (B), and 0.936 (R'). The dimensionless separation factor R_L confirms that this isotherm is favorable because its measured value is between zero and one. The Langmuir model is based on the following assumptions: the equivalence of all adsorption sites, the non-dependence of the adsorption energy on the surface coverage rate, the absence of interactions between adsorbed and adjacent species on the surface, the reversibility of adsorption, which is essentially physical, and the uniformity of the solid surface.

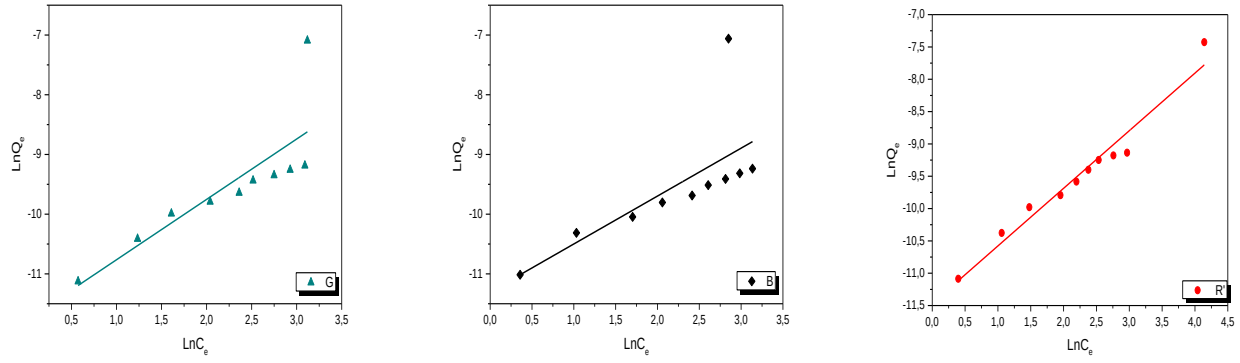

Fig 17. Linearization of the Freundlich isotherm for conventional sorption of TPC on G, B, and R' adsorbents at room temperature.

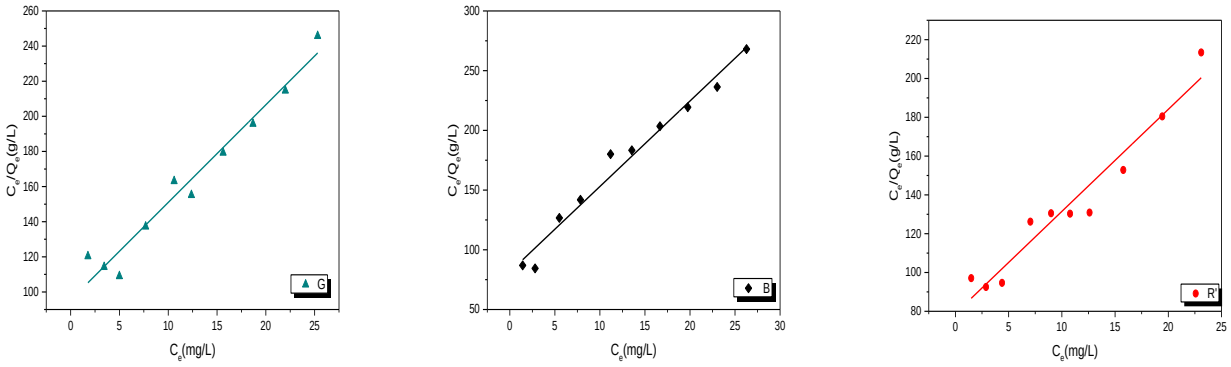

Fig 18. Linearization of the Langmuir isotherm for conventional sorption of TPC on G, B, and R' adsorbents at room temperature.

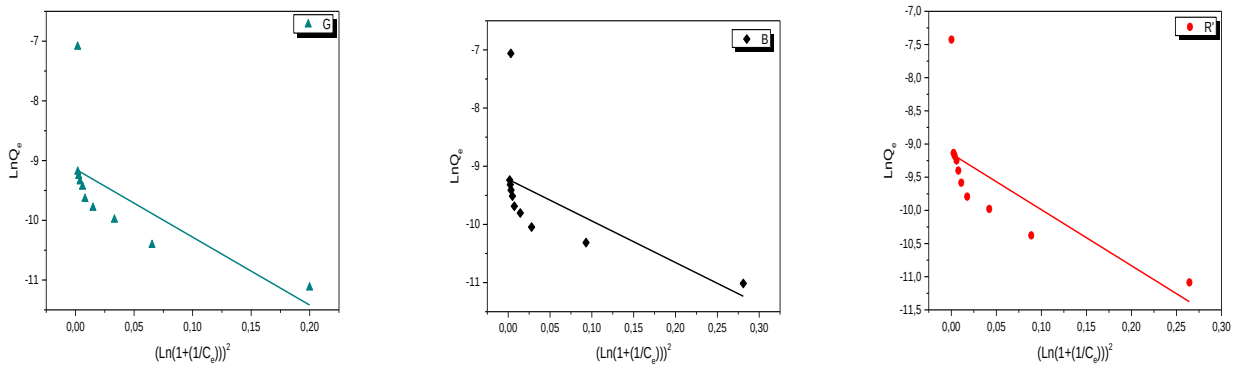

Fig 19. Linearization of the Langmuir isotherm for conventional sorption of TPC on G, B, and R' adsorbents at room temperature.

Table 9. Parametric values of the models chosen for this study for the conventional adsorption of TPC from the olive mill wastewater by the three adsorbents.

	Adsorbents →	**G**	**B**	**R'**
Isotherm models ↓	**Parameters ↓**			
Freundlich	K_F **(L/mg)**	$7.702\ 10^{-6}$	$12.354\ 10^{-6}$	$10.451\ 10^{-6}$
	1/*n*	1.011	0.802	0.891
	r^2	0.644	0.453	0.957
Langmuir	K_L **(L/mg)**	0.058	0.088	0.067
	Q_{max} **(mg/g)**	0.180	0.140	0.190
	R_L	0.105	0.072	0.093
	r^2	0.957	0.972	0.936
Dubinin-Radushkevich	q_{max} **(mg/g)**	$10.696\ 10^{-5}$	$9.847\ 10^{-5}$	$10.667\ 10^{-5}$
	β' **(mol/kJ)^2**	1.854	1.164	1.375
	E_D **(kJ/mol)**	0.519	0.655	0.603
	r^2	0.385	0.298	0.464

However, the Freundlich isotherm provided a better match for the adsorption of TPC on R' soil because the determination coefficient r^2 is closest to unity (0.957). The value of the parameter (1/*n*) is between 0 and 1, indicating that TPC adsorption onto soil *R'* is favorable. The classification of these isotherms (L) confirms the slowness of the process because the attractive forces between the adsorbed molecules are weak.

4. Conclusion

The objective of this study was to find the optimal conditions for the removal of TPC from olive mill wastewater. Our experimental trials aimed to test the adsorption capacity of natural soils under conventional and microwave conditions. They were chosen to reduce costs and to simplify the treatment process of olive mill wastewater.

The results showed that the retention of the TPC is faster under microwave irradiation conditions than under conventional conditions. Equilibrium is reached after 5-10 seconds in contrast to conventional sorption, where the shortest equilibrium time is 2 hours.

The results of the kinetic study for all the pollutants show that the retention is very fast under microwave irradiation conditions (almost instantaneous). The linear regressions showed that the kinetics is controlled by the pseudo-second-order model. This is confirmed by the values of the coefficients of determination corresponding to each model.

The sorption isotherm study showed that the experimental data are well reproduced by the Langmuir model for the G, B adsorbents ($r^2 > 0.95$) and by the Freundlich model for the R adsorbent ($r^2 \geq 0.96$). The Langmuir model can also be described also on R' soil because $r^2 = 0.94$. The dimensionless separation factor (R_L) confirms the application of this last model, as it is between zero and one, thus favorable.

Given these results, it is concluded that the conventional sorption process is slow and better compared to the microwave irradiation sorption, which is more than fast. The removal rate of TPC is acceptable under conventional conditions because it reaches 71% in the soil, noted G. The removal of TPC by conventional sorption is better than sorption under microwave irradiation.

Funding Support

There is no funding source to declare.

Ethical Statement

This study does not contain any studies with human or animal subjects performed by any of the authors.

Conflict of Interest

The authors declare no conflicts of interest.

Data Availability Statement

Not applicable.

.

References

1. Iboukhoulef H, Douani R, Amrane A, et al. Heterogenous Fenton like degradation of olive Mill wastewater using ozone in the presence of BiFeO3 photocatalyst. *J Photochem Photobiol A Chem.* 2019. https://doi.org/10.1016/j.jphotochem.2019.112012
2. Tchakala I, Kodom T, Alfa-Sika MS-L, et al. Traitement d'une eau naturelle polluée par adsorption sur du charbon actif (CAK) préparé à partir de tourteaux de karité. *Déchets Sci Tech*. 2016;(72).
3. Zidane F, Rhazzar A, Blais JF, et al. Contribution à la dépollution des eaux usées de textile par électrocoagulation et par adsorption sur des composés à base de fer et d'aluminium. *Int J Biol Chem Sci*. 2011;5:1727-1745.
4. Aliakbarian B, Casazza AA, Perego P. Kinetic and isotherm modeling of the adsorption of phenolic compounds from olive mill wastewater onto activated carbon. *Food Technol Biotechnol*. 2015;53:207–214.
5. Al Mallah K, Asma OJ, Abu Lail NI. Olive mills effluent (OME) wastewater post-treatment using activated clay. *Sep Purif Technol*. 2012;20:225-234.
6. Achak M, Hafidi A, Ouazzani N, et al. Low cost biosorbent "banana peel" for the removal of phenolic compounds from olive mill wastewater: Kinetic and equilibrium studies. *J Hazard Mater*. 2009;166:117–125.
7. Achak M, Hafidi A, Mandi L, et al. Removal of phenolic compounds from olive mill wastewater by adsorption onto wheat bran. *Desalin Water Treat*. 2014;52:2875-2885.
8. NI ISO 5667-3. Qualité de l'eau - Echantillonnage. Partie 03: Conservation et manipulation des échantillons d'eau. 2012.

9. NF T 90-008. Qualité de l'eau - Détermination du pH. 2001.
10. NF EN 27888. Qualité de l'eau - Détermination de la conductivité électrique. 1994.
11. Box JD. Investigation of the Folin–Ciocalteu phenol reagent for the determination of polyphenolic substances in natural waters. *Water Res*. 1983;17:511-525.
12. NF ISO 10390. Qualité du sol - Détermination du pH. 2005.
13. Babić BM, Milonjić SK, Polovina MJ, et al. Point of zero charge and intrinsic equilibrium constants of activated carbon cloth. *Carbon*. 1999;37:477–481.
14. JCPDS. Diffraction data CD-ROM. International Centre of Diffraction Data, Newtown Square P.A.; 2000.
15. Mathon MH. Caractérisation des textures par diffraction neutronique. *Collection SFN*. 2008;9:49–64.
16. Wang X, Wang J, Zhang J. Comparisons of three methods for organic and inorganic carbon in calcareous soils of northwestern China. *PLoS One.* 2012;7(8):e44334.
17. Mathieu C, Pieltain F. Analyse chimique des sols: méthodes choisies. Paris: Lavoisier, TEC & DOC; 2003. ISBN: 2-7430-0620-X.
18. Brunauer S, Emmett PH. The use of low temperature Van der Waals adsorption isotherms in determining surface areas of various adsorbents. *J Am Chem Soc*. 1937;59:2682-2689.
19. Srivastava VC, Swamy MM, Mall ID, et al. Adsorptive removal of phenol by bagasse fly ash and activated carbon: Equilibrium, kinetics and thermodynamics. *Colloids Surf A Physicochem Eng Asp*. 2006;272:89-104.
20. Li W, Zhang L, Peng J, et al. Tobacco stems as a low cost adsorbent for the removal of Pb(II) from wastewater: Equilibrium and kinetic studies. *Ind Crops Prod*. 2008;28:294-302.
21. Martins AE, Pereira MS, Jorgetto AO, et al. The reactive surface of Castor leaf (Ricinus communis L.) powder as a green adsorbent for the removal of heavy metals from natural river water. *Appl Surf Sci*. 2013;276:24–30.
22. Weber WJ, Morris JC. Kinetics of adsorption on carbon from solution. *J Sanit Eng Div Am Soc Civ Eng*. 1963;89:31–60.
23. Hameed BH, Tan IAW, Ahmad AL. Adsorption isotherm, kinetic modeling and mechanism of 2,4,6-trichlorophenol on coconut husk-based activated carbon. *Chem Eng J.* 2008;144:235–243.
24. Hgag SW, Abdel Moniem SMA, Ali MEM, et al. Isotherm models for metal removal using modified graphene. *Egypt J Chem.* 2024;67:245-252.
25. Fayoud N, Alami Younssi S, Tahiri S, et al. Etude cinétique et thermodynamique de l'adsorption de bleu de méthylène sur les cendres de bois. *J Mater Environ Sci*. 2015;6:3295-3306.
26. Erhayem M, Al-Tohami F, Mohamed R, et al. Isotherm, kinetic and thermodynamic studies for the sorption of mercury (II) onto activated carbon from *Rosmarinus officinalis* leaves. *Am J Anal Chem*. 2015;6:1-10.
27. Kedi ABB. Fonctionnement des phosphatases dans les sols tropicaux: Influence de la composition organo-minérale sur l'expression de l'activité enzymatique [dissertation]. Montpellier: SupAgro & Univ. of Cocody-Abidjan; 2011.
28. Oertli JJ. Soil fertility. In: Chesworth W, ed. *Encyclopedia of Soil Sciences. Springer*; 2008:656-668.
29. Calvet R. Le sol: propriétés et fonctions. Tome 1: Constitution et structure, phénomènes aux interfaces. Paris: Dunod; 2003.
30. Awaleh MO, Farah IG, Adawe LF, et al. Potentialité d'utilisation d'argiles Djiboutiennes dans l'industrie céramique. *SciLib Mersenne*. 2014;6:141106.
31. Böke H, Akkurt S, Özdemir S, et al. Quantification of CaCO3–CaSO3·0.5H2O–CaSO4·2H2O mixtures by FTIR analysis and its ANN model. *Mater Lett.* 2004;58:723–726.
32. Filip Z, Demnerova K. Humic substances as a natural factor lowering ecological risk in estuaries. In: Linkov I, et al., eds. Springer; 2007:343–353.
33. Lee BS, Lin HP, Chan JCC, et al. A novel sol-gel-derived calcium silicate cement with short setting time for application in endodontic repair of perforations. *Int J Nanomedicine*. 2018;13:261-271.
34. Madejová J. FTIR techniques in clay mineral studies. *Vib Spectrosc*. 2003;31:1–10.
35. Ndzana GM, Huang L, Wang JB, et al. Characteristics of clay minerals in soil particles from an argillic horizon of Alfisol in central China. *Appl Clay Sci.* 2018;151:148-156.
36. Saikia BJ, Parthasarathy G. Fourier transform infrared spectroscopic characterization of kaolinite from Assam and Meghalaya, Northeastern India. *J Mod Phys*. 2010;1:206-210.
37. Biglari H, Afsharnia M, Javan N, et al. Phenol removal from aqueous solutions by adsorption on activated carbon of miswak's root treated with KMnO4. *Iran J Health Sci*. 2016;4:20-30.
38. Buran TJ, Sandhu AK, Li Z, et al. Adsorption/desorption characteristics and separation of anthocyanins and polyphenols from blueberries using macroporous adsorbent resins. *J Food Eng*. 2014;128:167–173.
39. Chaudhary N, Balomajumder C. Optimization study of adsorption parameters for removal of phenol on aluminum impregnated fly ash using response surface methodology. *J Taiwan Inst Chem Eng*. 2014;45:852–859.
40. Djebbar M, Djafri F, Bouchekara M, et al. Adsorption of phenol on natural clay. *Appl Water Sci.* 2012;2:77–86.
41. Karbowiak T, Mansfield AK, Barrera-García VD, et al. Sorption and diffusion properties of volatile phenols into cork. *Food Chem*. 2010;122:1089-1094.
42. Numbonui Ghogomu J, Tsemo Noufame D, Buleng Njoyim Tamungang A, et al. Adsorption of phenol from aqueous

solutions onto natural and thermally modified kaolinitic materials. Int J Biol Chem Sci. 2014;8:2325-2338.
43. Thawornchaisit U, Pakulanon K. Application of dried sewage sludge as phenol biosorbent. *Biotechnol*. 2007;98:140–144.
44. Qadeer R, Rehan AH. A study of the adsorption of phenol on activated carbon from aqueous solutions. *Turk J Chem. 2002;26:357-361.*
45. El Gaidoumi A, Chaouni Benabdallah A, Lahrichi A, et al. Adsorption du phénol en milieu aqueux par une pyrophyllite Marocaine brute et traitée. *J Mater Environ Sci*. 2015;6:2247-2259.
46. Garg VK, Kumar R, Gupta R. Removal of malachite green dye from aqueous solution by adsorption using agro-industry waste: A case study of *Prosopis cineraria*. *Dyes Pigm.* 2004;62:1–10.
47. Aarfane A, Salhi A, El Krati M, et al. Etude cinétique et thermodynamique de l'adsorption des colorants Red195 et Bleu de méthylène en milieu aqueux sur les cendres volantes et les mâchefers. *J Mater Environ Sci*. 2014;5:1927-1939.
48. Uddin MT, Islam MS, Abedin MZ. Adsorption of phenol from aqueous solution by water hyacinth ash. *ARPN J Eng Appl Sci.* 2007;2:11-17.
49. Datta C, Dutta A, Dutta D, et al. Adsorption of polyphenols from ginger rhizomes on an anion exchange resin Amberlite IR-400 – Study on effect of pH and temperature. *Procedia Food Sci*. 2011;1:893–899.
50. Foo KY, Hameed BH. Recent developments in the preparation and regeneration of activated carbons by microwaves. *Adv Colloid Interface Sci.* 2009;149:19–27.
51. Foo KY, Hameed BH. Microwave-assisted regeneration of activated carbon. *Bioresour Technol*. 2012;119:234–240.
52. Arellano-Cárdenas S, Gallardo-Velázquez T, Osorio-Revilla G, et al. Adsorption of phenol and dichlorophenols from aqueous solutions by porous clay heterostructure (PCH). *J Mex Chem Soc*. 2005;49:287-291.
53. Chen Y, Ye WM, Zhang K. Factors affecting phenol adsorption on clay-solidified grouting curtain. *J Cent South Univ Technol.* 2011;18:854-858.
54. Silva MMF, Oliveira MM, Avelino MC, et al. Adsorption of an industrial anionic dye by modified-KSF-montmorillonite: Evaluation of the kinetic, thermodynamic and equilibrium data. *Chem Eng J.* 2012;203:259–268.
55. Ho YS, McKay G. The kinetics of sorption of divalent metal ions onto sphagnum moss peat. *Water Res*. 2000;34:735-742.